THE JOURNAL OF PHYSICAL CHEMISTRY B

Article

Cite This: J. Phys. Chem. B 2019, 123, 2623−2635

pubs.acs.org/JPCB

Role of Diffusion in Unfolding and Translocation of Multidomain Titin I27 Substrates by a Clp ATPase Nanomachine

Abdolreza Javidialesaadi,[†,§] Shanice M. Flournoy,[‡] and George Stan*[,†]

[†]Department of Chemistry, University of Cincinnati, Cincinnati, Ohio 45221, United States

[‡]Department of Chemistry, Virginia State University, Petersburg, Virginia 23806, United States

Supporting Information

ABSTRACT: Degradation of multidomain substrate proteins (SPs) by AAA+ nanomachines takes place processively from the tagged terminal. Ring-shaped ATPase components, such as ClpY, apply repetitive mechanical forces to effect domain unfolding and translocation of polypeptide segments through a narrow central channel. We study these mechanisms through atomistic Langevin dynamics simulations of C-terminal-tagged SPs in allosteric ClpY cycles. We find that monomeric SPs are processed through single unfolding pathways and fast timescales, whereas multimeric SPs involve branched pathways and slower timescales. These distinct mechanisms are attributed to the slower rotational diffusion of the C-terminal domain in multidomain SPs that hinders access to the soft mechanical direction. In the geometry specific to laser optical tweezers experiments, involving a restrained SP N-terminal, a single unfolding pathway is found for both monomeric and tetrameric SPs as pulling is applied along the N−C direction. Non-native interactions modulate unfolding of unrestrained monomers by weakening the C-terminal interface but do not contribute significantly to unfolding of restrained SPs. On the basis of these results, we propose that the interplay of restricted SP dynamics and ATPase kinetics underlies partitioning of multidomain SPs into completely degraded products and undegraded fragments comprising folded domains.

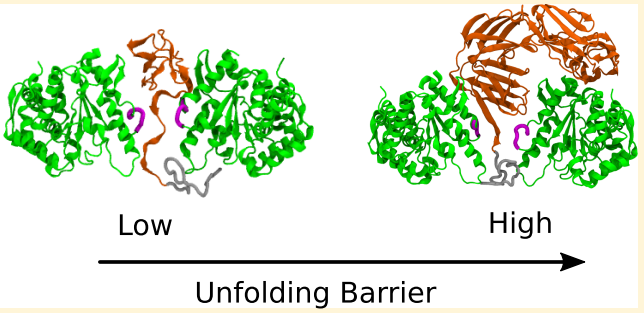

INTRODUCTION

Proteins targeted for degradation are processed by a complex machinery, which integrates unfolding and peptidase components, such as bacterial caseinolytic proteases (Clp) and the eukaryotic 26S proteasome. The structurally simpler Clp biological nanomachines comprise one or two AAA+ (ATPases associated with various cellular activities) hexameric rings which dock the barrel-like peptidase compartment in an axially aligned complex to facilitate polypeptide translocation through the narrow central channel. Substrate proteins (SPs) are recognized by the Clp nanomachine through a degron signal, such as the 11-mer SsrA peptide, that is covalently attached at the C-terminal of the SP.[1] During nonconcerted allosteric cycles of the Clp nanomachine, a set of conserved central channel loops of the AAA+ ring effects SP unfolding through repetitive application of mechanical force and enables up to four translocation steps of 1 nm each per cycle.[2−4] Through these mechanisms, SPs are processively unfolded and translocated starting with their tagged terminal region.[5]

Degradation rates of fusion SPs comprising multiple folded domains are determined by competing mechanisms of binding-release, unfolding and refolding of individual domains, and translocation of polypeptide segments.[3,6−8] The unfolding of each SP domain is strongly dependent on its mechanical stability near the terminal to which force is being applied.[5,9] In accord with the local stability model, higher degradation rates are observed for domains with weak mechanical resistance, such as HaloTag (helical structure), compared with domains with strong mechanical resistance, such as titin I27 (β-sheet) or green fluorescent protein (GFP, β-barrel). In addition, force directionality plays an important role in the unfolding of domains with mechanical anisotropy, such as titin I27, which leads to slow unfolding timescales associated with strong mechanical directions. For multidomain SPs, interdomain interactions can provide a stabilizing effect against unfolding. The inability to complete the requisite successive unfolding events within timescales associated with the degradation of unfolded polypeptide tracks may result in partial degradation or stalling the degradation process altogether. Experimental studies revealed that a dihydrofolate reductase (DHFR)-barnase SP is completely protected against degradation when DHFR is stabilized through the tightly binding ligand methraxate.[5] Studies of the degradation of tandems comprising 1−3 I27 domains highlight the release of partially degraded species that contain a subset of folded domains and unfolded tails with length consistent with the distance to the peptidase compartment.[6] The degradation process may also stall in the presence of a stop signal, a mechanism which underlies a post-

Received: October 22, 2018
Revised: January 24, 2019
Published: January 25, 2019

DOI: 10.1021/acs.jpcb.8b10282
J. Phys. Chem. B 2019, 123, 2623−2635

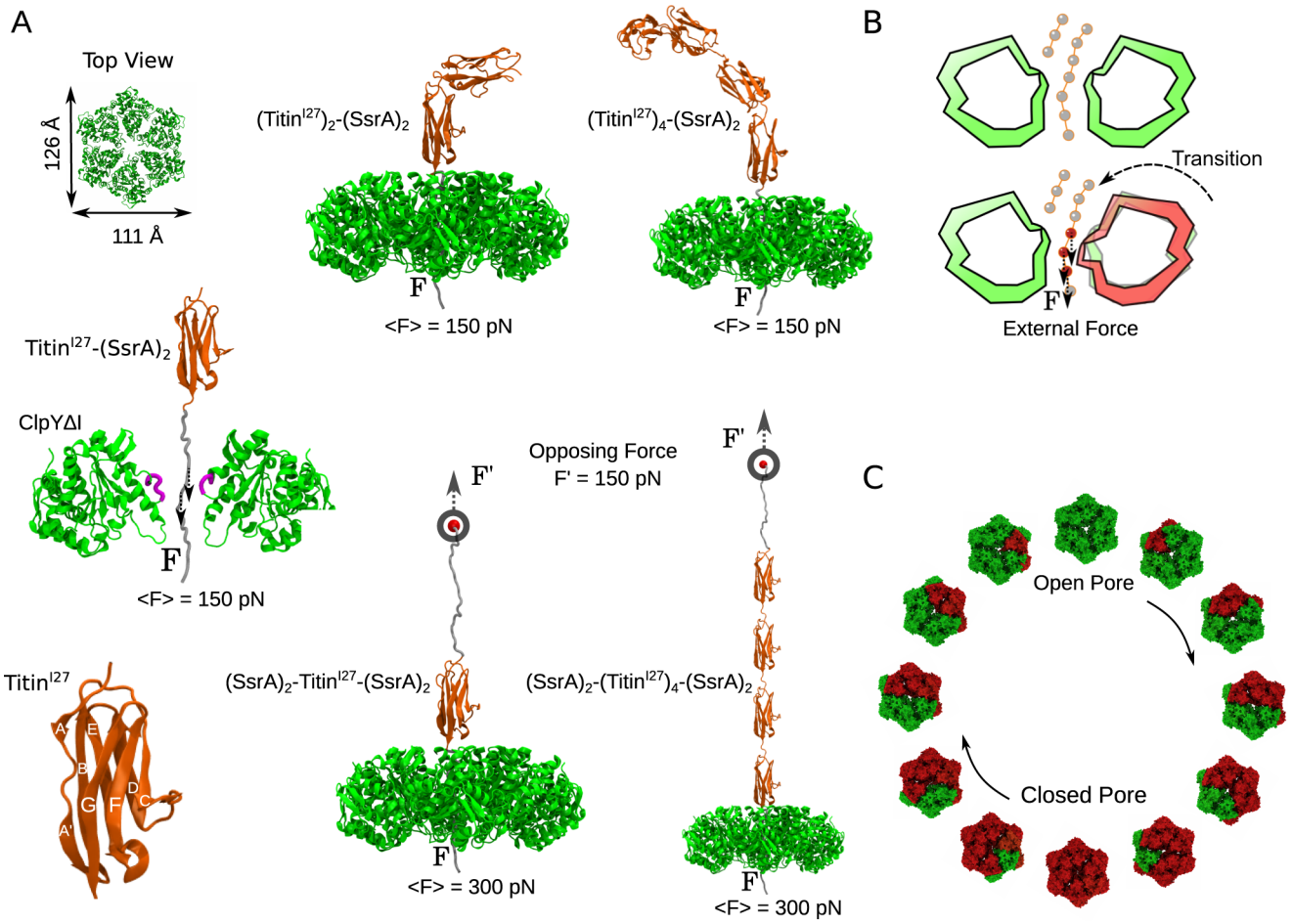

Figure 1. Remodeling of I27 tandem substrates by ClpYΔI. (A) Simulations of ClpYΔI-mediated protein unfolding and translocation involve unrestrained (top panels) or restrained (bottom panels) SP N-terminals that mimic cellular mechanisms or single-molecule pulling experiments, respectively. During ATP-driven cycles of ClpYΔI (green and gray), conserved central channel loops (purple) engage the SP and apply mechanical force along the pore axis. SP tandems include 1, 2, or 4 titin I27 domains (orange) and $(SsrA)_2$ peptides (gray). The β-sheet structure of the I27 domain is also indicated. In our simulation, an external force is applied onto the SP amino acids located within the ClpY channel during open → closed transitions and in restrained geometries an opposing force is applied to the N-terminal of the SP (see Methods). (B) Schematic view of conformational changes during the sequential ClpY cycle. During each ATP-hydrolysis step, one subunit undergoes a conformational transition between its open (green) and closed (red) pore configuration and promotes SP unfolding and translocation. (C) Schematic representation of the ClpY cycle. Sequential subunit conformational transitions between open (green) and closed (red) pore configurations are implemented in the clockwise direction. Visual molecular dynamics[54] was used to render molecular graphics.

translational regulation process to release partial degradation fragments with new biological activity, such as for transcription factors.[10−20] For example, the grip of the SP by the AAA+ machine becomes too weak upon encountering a low complexity sequence along the polypeptide chain, such as the glycine-rich region of p105 and p100 precursors of NF-κB, which stalls the proteolytic process and releases p50 and p52 fragments,[16] and of the τ form of the ATP-binding clamp loader subunit DnaX to yield ClpXP-mediated release of the shorter γ form.[21] A distinct type of stop signal is present in knotted proteins. Theoretical and computational studies indicate that although forced translocation of knotted polymers and proteins through narrow pores can be achieved through displacement of the knot toward the free end, translocation of tightened knots requires the crossing of large energy barriers.[22−28] Biophysical and biochemical experiments revealed that C-terminal pulling of the 3_1-knotted protein MJ0366 from *M. jannaschii* by the ClpXP protease results in complete translocation through knot sliding to the free N-terminal and knot tightening when a long unstructured linker is attached to the N-terminal, however, it results in stalled degradation when a stabilizing folded GFP domain is added at the N-terminal.[29]

Bulk mechanical properties of multidomain SPs have been studied extensively using single-molecule approaches, such as laser optical tweezers (LOT) or atomic force microscopy (AFM), which restrict the application of force to the direction of N−C terminals and therefore probe mechanical resistance along a specific direction. These studies reveal statistical effects of unfolding of identical domains, such as the requirement of larger critical unfolding forces for the single domain compared with a homogeneous multidomain SP.[30] In LOT experiments of Clp-mediated unfolding, a distribution of dwell times between unfolding events was reported for SPs comprising multiple folded domains.[7,31−35] These experiments revealed unfolding pathways consistent with the mechanical strength of the N−C direction and showed that the Clp-mediated force has a lower bound of ≃20 pN resulting in a mechanical work of approximately $5k_BT$.

DOI: 10.1021/acs.jpcb.8b10282
J. Phys. Chem. B 2019, 123, 2623−2635

Table 1. Summary of Implicit Solvent Simulations of Allosteric and Nonallosteric ClpYΔI Performed

substrate protein	geometry	ClpYΔI	N_{traj}[a]	N_{unfold}[b]	$\langle\tau_u\rangle(\tau)$[c]
I27−$(SsrA)_2$	unrestrained	nonallosteric	12	0	
I27−$(SsrA)_2$	unrestrained	allosteric	24	24	112 ± 13
$(I27)_2$−$(SsrA)_2$	unrestrained	allosteric	12	12	271 ± 43
$(I27)_4$−$(SsrA)_2$	unrestrained	allosteric	17	6	377 ± 44
$(SsrA)_2$−I27−$(SsrA)_2$	restrained[d]	allosteric	36	25	277 ± 29
$(SsrA)_2$−$(I27)_4$−$(SsrA)_2$	restrained	allosteric	23	13	316 ± 42

[a]The number of simulation trajectories performed. The duration of each trajectory corresponds to 500 Clp ATPase cycles of τ = 120 ps for a total of 60 ns. [b]Number of trajectories in which initial unfolding of the C-terminal I27 domain is observed. The unfolding criterion is indicated in the Methods section. [c]Average unfolding time and standard error in the mean expressed in the number of cycles τ. [d]An opposing force with magnitude 150 pN is applied at the SP N-terminal of the SP during the simulation.

Mechanical resistance of the titin I27 domain to application of force is controlled by the strong A′−G interstrand interface. AFM experiments, in which force is applied along the N−C direction parallel to the A′ and G strands, reveal that I27 is able to withstand forces up to ≃200 pN.[36,37] In accord with experimental results, computer simulations of bulk mechanical pulling indicate that the unfolding mechanism involves the loss of contacts between A and B strands followed by shearing of the A′−G interface.[38−44] Given the dominant role of the A′−G interface, the consistency between simulation studies is not surprising, however, it is notable that the agreement holds over multiple length scales associated with diverse I27 domain representations ranging from native-centric coarse-grained models[41−44] to implicit[39−41] and explicit solvent[38] atomistic descriptions. In particular, the EEF1 implicit solvent model,[45,46] which is used in this study, reveals, in close agreement with AFM studies, that the unfolding pathway includes a metastable intermediate resulting from the removal of the A strand followed by removal of A′−G contacts.[39]

Prior computational studies focused on single-domain SP unfolding and translocation mechanisms using model pore or coarse-grained representation of the Clp ATPase structure and highlighted the role of local mechanical stability and anisotropy of the SP in Clp-mediated degradation.[41,44,47−53] Our coarse-grained studies of I27 unfolding at the surface of a nonallosteric ClpY ring indicate that ClpY plasticity yields propensity for specific unfolding mechanisms.[52] The ATP-bound "open" pore configuration of ClpY favors orientation of the I27 β-sheet registry in the direction perpendicular to the ClpY axis, and that SP unfolding takes place along a soft mechanical direction through unzipping A′−G interstrand contacts. The ADP-bound "closed" pore configuration selects I27 orientations with the β-sheet registry nearly parallel to the pore axis, which favors a shearing unfolding mechanism.

In this paper, we introduce an atomistic model of the Clp−SP system that enables us to probe the microscopic details of SP unfolding and translocation mechanisms over the long timescales associated with these actions. We focus on SP tandems comprising up to four titin I27 domains (Figure 1), which provide insight into the remodeling of mechanically anisotropic domains. Our simulations contrast in vivo action, in which the SP C-terminal is tagged and the N-terminal is unrestrained, and the LOT-like setup, in which an opposing force is applied at the N-terminal. We find that the unrestrained single-domain SP is immobilized in an orientation that favors the unzipping mechanism, and unfolding proceeds on a fast timescale and with high efficiency. By contrast, rotational flexibility of multidomain SPs is hindered and results in significantly less efficient unfolding along two pathways that involve either unzipping or shearing of the C-terminal SP. Non-native interactions within the SP modulate these actions by weakening the A′−G interface in the unrestrained SP, while having only a small contribution to the mechanism involving the restrained SP.

METHODS

Implicit Solvent Model of ClpYΔI and Substrate Proteins. To probe atomic level interactions between the ATPase and the substrate in a computationally efficient approach, we describe the ClpYΔI−SP system by using the EEF1 implicit solvent model.[45,46] Protein−protein interactions described using this transferable force field were found to be in agreement with explicit solvent atomistic simulations for the GroEL−rhodanese system.[55] In our studies, SPs comprise an $(SsrA)_2$ degradation tag (SsrA sequence AANDENYALAA) covalently attached at the C-terminal (unrestrained geometries) or at both the C- and N-terminals (restrained geometries) of tandems of 1, 2, or 4 titin I27 domains (Table 1). Although a single SsrA tag is sufficient for SP engagement by the Clp ATPase, a longer peptide enables us to probe a larger initial separation between the C-terminal-folded domain and Clp and to avoid biased initial configurations. The initial SP conformations are obtained by using model-built SsrA coordinates corresponding to an extended structure of the peptide and the crystal structure of the human I27 domain with protein data bank (PDB) ID 1TIT.[56] In the initial configuration of the ClpYΔI−SP system, the ClpY ATPase is centered around the origin such that its pore axis is aligned with the z-axis, and the distal side corresponds to positive z values. Initial configurations of multidomain SPs are generated by performing equilibrium bulk simulations and are selected to avoid steric overlap with the Clp ATPase. The relative orientation of the SP and Clp ATPase is obtained by aligning the largest principal axis of inertia of the C-terminal I27 domain with the ClpY pore axis. The center of mass of the I27 domain is initially positioned on the proximal side of the nanomachine, along the z-axis, at $z \approx -30$ Å, such that part of the $(SsrA)_2$ tag is located within the ClpY pore. Distinct initial configurations are generated by random SP rotations about the z-axis. We use the CHARMM program[57] and Extreme Science and Engineering Discovery Environment (XSEDE) supercomputer resources[58] to perform the Langevin dynamics simulations at T = 300 K, with a friction coefficient of 5 ps^{-1} and a time step of 2 fs.

ClpYΔI Allosteric Motions. To access the ms-s timescales associated with the Clp ATPase motions, we describe conformational transitions of individual subunits by using the targeted molecular dynamics[59] approach which samples

DOI: 10.1021/acs.jpcb.8b10282
J. Phys. Chem. B 2019, 123, 2623−2635

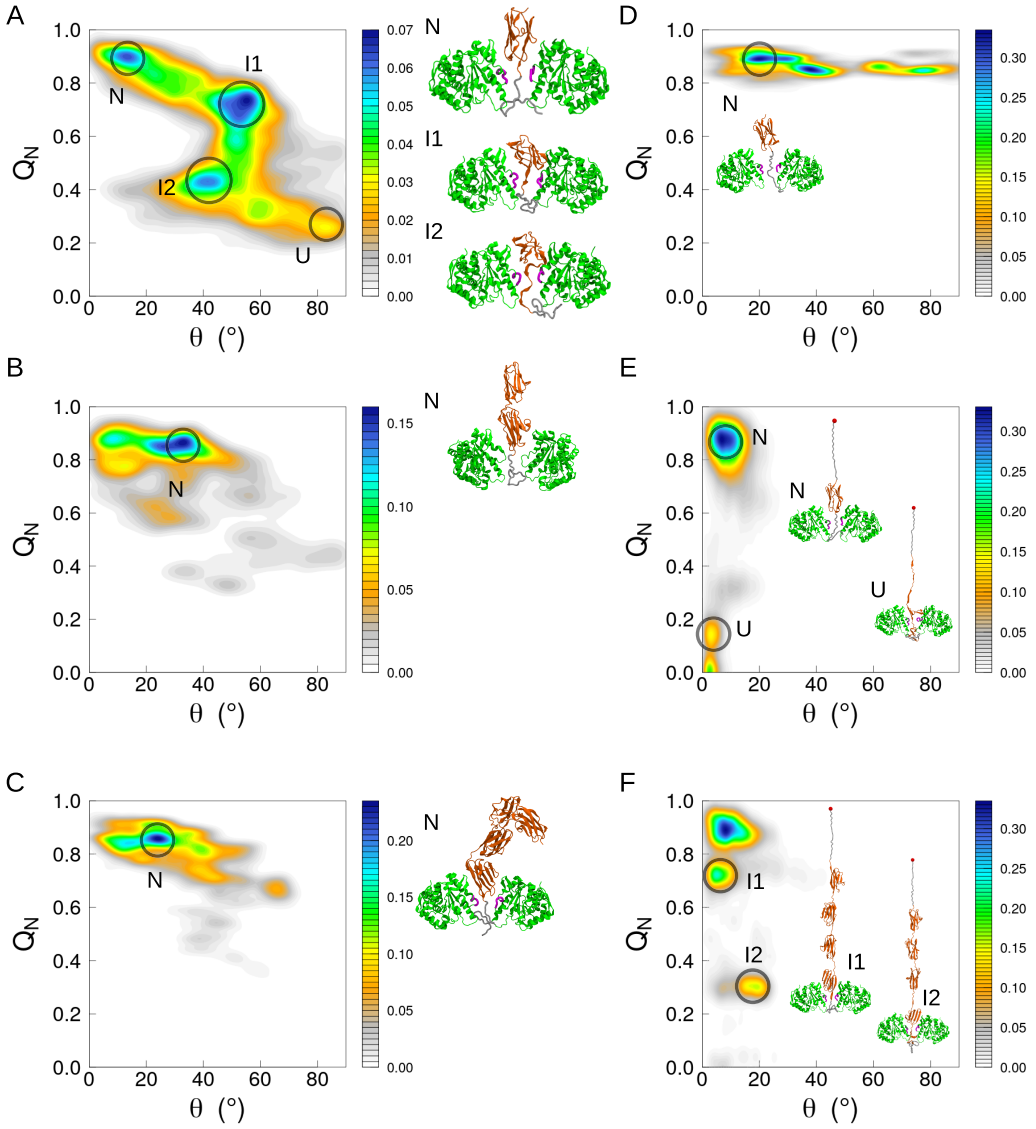

Figure 2. Direction-dependent unfolding mechanisms of multidomain SPs mediated by ClpYΔI. Probability density maps of the fraction of native contacts of the C-terminal I27 domain, Q_N, and the polar angle θ between its first principal axis and the ClpYΔI pore axis are shown for the (A) monomeric (B) dimeric, and (C) tetrameric SPs in the unrestrained geometry in allosteric cycles of ClpYΔI. Corresponding maps are shown for (D) unrestrained monomeric SP and nonallosteric ClpYΔI and restrained (E) monomeric and (F) tetrameric SP and allosteric ClpYΔI. The conformational states corresponding to the largest densities and representative structures of the C-terminal I27 domain conformations are highlighted.

pathways that reduce the root mean square deviation between the initial and final conformations. We note that this approach yields good results for nanomachines such as GroEL whose subunit motions can be described by a small number of collective variables (CVs), such as low-frequency normal modes[60−62] or principal components.[63] More complex transitions require biasing techniques which may involve multiple CVs.[64] The Clp ATPase cycle is described through transitions between open and closed pore conformations, corresponding to *Escherichia coli* ClpY crystal structures with PDB IDs 1DO2 (open pore) and 1DO0 (closed).[65] As the I-domains (residues 111−242) of ClpY subunits are not modeled in our simulations, we represent each ClpY subunit using two chains. Each hemicycle consists of six sequential transitions of individual ClpY subunits, which undergo conformational changes between their open and closed state configurations. The subunit that undergoes the first transition in the hemicycle is selected at random. Subsequent transitions follow a clockwise intraring order as observed from the proximal side of ClpY. During each one-subunit transition, the center of mass of the other five subunits is restrained to the current position.

External Repetitive Force Coupled with Allosteric Motions. To accelerate SP unfolding and translocation, we apply an external pulling force, during the open → closed hemicycle, to the SP segment that is transiently located within the ClpY pore at the beginning of each single subunit transition. The magnitude of the external force obeys the Gaussian distribution with average 150 pN (unrestrained geometry) or 300 pN (restrained) and a standard deviation of 10 pN. The force is applied in the z-direction, and it is uniformly distributed on heavy atoms of the SP amino acids which are instantaneously located within the ClpY pore, i.e., $|z_i - \langle z_{loop} \rangle| < 5$ Å, where z_i is the location of the SP heavy atom

DOI: 10.1021/acs.jpcb.8b10282
J. Phys. Chem. B 2019, 123, 2623−2635

and $\langle z_{loop} \rangle$ is the average position of the ClpY pore loops evaluated at the beginning of each transition in the hemicycle. We find that the number of backbone atoms that are located in the confined region is about 20 atoms, therefore the applied force per atom has an average of ≃7.5 pN in the unrestrained geometry and ≃15 pN in the restrained geometry. In the restrained geometry, an opposing external force of 150 pN is applied onto the N-terminal such that the net external force has an average magnitude of 150 pN.

Nonallosteric ClpYΔI. To discriminate the effect of the external force on SP remodeling in the absence of allosteric motions of ClpY, we performed simulations in which no subunit conformational transitions are induced, and all Cα atoms of ClpY are restrained to their open state positions by using a harmonic restraint with a force constant of 2 kcal/(mol Å^2). An external force with an average magnitude of 150 pN is applied periodically to the SP segment located inside the confined region. In these simulations, the SP N-terminal is unrestrained.

Rotational Motion and Diffusion Coefficient. We characterize the orientation of the SP with respect to the ClpY pore axis by using the direction of the principal axis corresponding to the largest moment of inertia, I_1, of the C-terminal I27 domain. The reaction coordinate for the rotational motion is the angle θ formed by the unit vector $\vec{e}_1$ along the principal axis and the z axis. The apparent rotational diffusion coefficient D is estimated from the single-exponential fitting of the autocorrelation function $\langle \vec{e}_1(0) \cdot \vec{e}_1(t) \rangle = A \exp(-t/\tau_{rot})$. Using the relaxation time τ_{rot} of the autocorrelation function, the rotational diffusion coefficient is estimated by using $D = 1/(2\tau_{rot})$.

Fraction of Native and Non-Native Contacts. The fraction of native contacts Q_N is used to monitor unfolding of the C-terminal I27 domain, and it is calculated using $Q_N = (1/N_C)\sum_{i,j} \theta[\eta - |r_{ij}(t) - r_{ij}^0|]$, where N_C is the number of native contacts, $r_{ij}(t)$ is the minimum distance, at time t, between any two heavy atoms of residues i and j, with $|i - j| > 2$, and r_{ij}^0 is the corresponding minimum native distance. The cutoff distance for contacts is set to 6 Å. $\theta(x)$ is the Heaviside step function for which $\theta(x) = 1$ if $x \geq 0$ and $\theta(x) = 0$ if $x < 0$, with tolerance $\eta = 2$ Å. The fraction of non-native contacts (Q_{NN}) is calculated by using $Q_{NN} = N_{NC}/N_C$ where N_{NC} is the number of non-native heavy atom pairs identified using the 6 Å cutoff. The unfolding criterion used in our analysis requires that simultaneous conditions of the total and of the A′ strand fraction of native contacts be satisfied, $Q_N \leq 0.8$ and $Q_N^{(A')} \leq 0.5$. The unfolding time in each trajectory is identified as a first passage time, i.e., the first time when the unfolding criterion is satisfied.

RESULTS

Allosteric Conformational Transitions of ClpY ATPase Underlie Efficient Unfolding and Translocation Mechanisms of Substrate Proteins Comprising a Single I27 Domain. To probe the mechanism of substrate protein (SP) unfolding in allosteric cycles of the ClpY nanomachine, we developed a model involving sequential conformational transitions of Clp subunits that result in cyclical pore closing and opening (see Methods and Figure 1). These transitions are described using the targeted molecular dynamics approach,[59] which has been found to yield results consistent with experiments for biological nanomachines such as GroEL[66] and F1-ATPase.[67] Here, we consider the ClpYΔI structure, which lacks the auxiliary I domain specific to ClpY, therefore our results provide information that is more broadly representative of Clp ATPase nanomachines. In our molecular dynamics simulations, we contrast restrained and unrestrained SP geometries (Figure 1 and Table 1) that mimic setups present in single-molecule LOT experiments and in the cellular environment, respectively. To effectively access the long timescales associated with SP unfolding and translocation mediated by ClpY ATPases, the pulling forces due to the ClpY central channel loops are complemented by an external force along the ClpY pore axis that assists translocation (see Figure 1 and Methods). In LOT experiments,[7,31−35] the multidomain SP is tethered to an optically trapped bead, whereas the Clp ATPase is attached to a second bead. SP engagement by the Clp ATPase results in an interbead tension. The position of the beads is adjusted to maintain constant tension during the domain unfolding events, which increase the end-to-end distance of the SP. Our restrained simulations mimic this setup by including an opposing force at the SP N-terminal (Figure 1 and Methods).

As shown in Figure 2A, unfolding a single-domain SP in the unrestrained geometry involves a single pathway comprising two intermediate unfolding conformations. The first step, corresponding to the N → I1 transition, involves rotation of the largest principal axis of the I27 domain with respect to the ClpY pore axis by a large angle, $\theta \gtrsim 50°$. Reorientation of the I27 domain enables application of the pulling force due to the ClpY loops along the soft mechanical direction perpendicular to the A′−G interface which results in unfolding by unzipping of the interface contacts (Supporting Information Figure S1A and Movie S1). As shown in Table 1, this mechanism is highly efficient, with all 24 trajectories resulting in unfolding and translocation and the average unfolding time in these simulations corresponds to $\langle \tau_u \rangle \simeq 112\tau$, where $\tau = 120$ ps is the duration of one Clp cycle. Once the G strand is detached from the I27 core structure, SP translocation proceeds simultaneously with processive removal of successive C-terminal strands. Rapid translocation of the unraveled I27 strands indicates that the rate-limiting step of SP degradation is the initial unfolding of the A′−G interface. During the unfolding of the I27 core, corresponding to the I1 → I2 transition, the smaller folded fragment of I27 has slightly an increased rotational flexibility which allows it to sample a broad range of angles around $\theta \simeq 40°$ (Figure 2A). Nevertheless, the largest principal axis of the I27 fragment is maintained at nearly the same orientation with respect to the ClpY pore axis until unfolding is completed and during the final step in the unfolding process, I2 → U, its orientation is further tilted to lie perpendicular to the ClpY pore axis. These results indicate that the tilted orientation of the I27 fragment is the most favorable for removal of interstrand contacts, as the ClpY-mediated force is applied along the soft mechanical direction of the β-sheet registry.

To ascertain the effect of the pulling speed on our results, we performed additional Clp−SP simulations of the monomeric SP at lower speeds and on shorter timescales. Our results are obtained from simulations (Table 1) in which the effective pulling speed is estimated to be $v \simeq 1$ Å/ps by taking into account the 1 nm loop excursion per Clp subunit transition, the cycle duration of $\tau = 120$ ps and 12 transitions per cycle. This pulling speed is consistent with those in bulk mechanical pulling simulations using atomistic descriptions,[38] and it

DOI: 10.1021/acs.jpcb.8b10282
J. Phys. Chem. B 2019, 123, 2623−2635

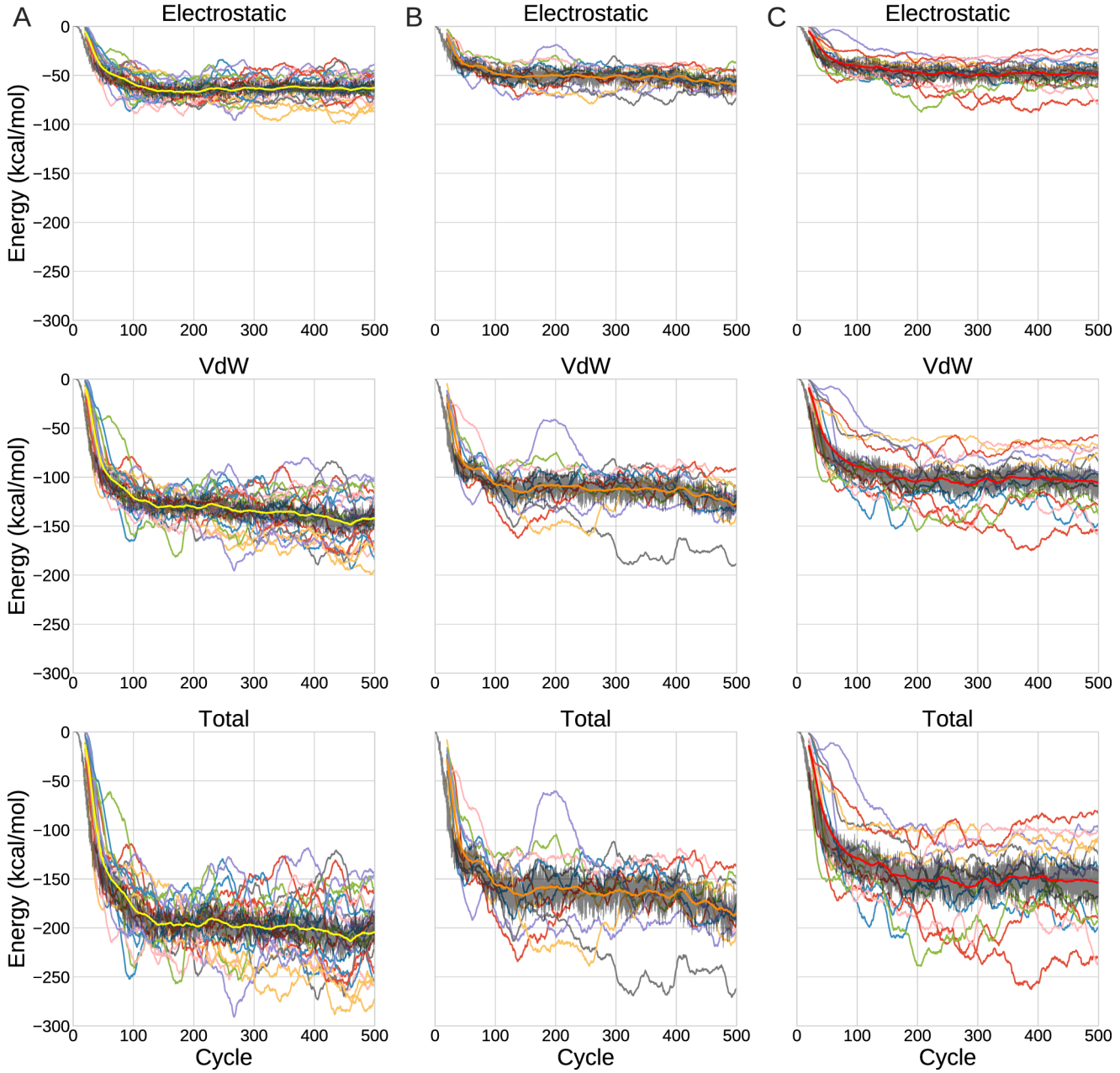

Figure 3. Interaction between the C-terminal I27 domain and ClpYΔI. Time series of electrostatic, van der Waals, and total interaction energies are shown for individual (thin curves) simulation trajectories of unrestrained (A) monomeric; (B) dimeric; and (C) tetrameric SPs in allosteric cycles of ClpYΔI. Ensemble-averaged interactions (thick curves) and standard errors in the mean (black lines) are superimposed onto each set of results.

represents the lowest speed for which we were able to obtain statistically relevant data. We performed additional simulations of unrestrained monomeric SPs with cycle durations of τ_1 = 600 ps and τ_2 = 6 ns, corresponding to $v_1 \simeq 0.2$ Å/ps and $v_2 \simeq 0.02$ Å/ps. In the former case, we observe initial unfolding events in 6 of the 7 simulation trajectories performed on a timescale $100\tau_1$. As shown in the Supporting Information Figure S2A, SP tilting occurs in all trajectories, and unfolding takes place through unzipping of A′−G contacts. In the latter case, unfolding is not observed in the 4 simulations with a cycle duration of τ_2 given the shorter timescale of $10\tau_2$, however, SP tilting occurs in all trajectories (Supporting Information Figure S2B). In the restrained geometry, we observe initial unfolding events in 7 of the 10 simulations with cycle duration of τ_1 and timescale of $100\tau_1$. In this geometry, unfolding occurs through a shearing mechanism, and the SP has limited rotational flexibility (Supporting Information Figure S2C). Overall, we conclude that the results of simulations presented in this study (Table 1) are consistent with those at lower pulling speeds.

Hindered Rotational Diffusion of Multidomain I27 SPs Results in Slower Unfolding through Multiple Pathways. We next consider the Clp-mediated processing of multidomain SPs obtained by covalently linking two or four I27 domains (see Methods), and we compare the unfolding and translocation mechanisms of the C-terminal I27 domain with those of single-domain SPs. As shown in Table 1, unfolding is observed in all 12 trajectories of the dimeric SP, and in 6 of 17 trajectories of the tetrameric SP and the associated unfolding times (see Methods) are $\langle \tau_u \rangle \simeq 271\tau$ for the dimer and $\langle \tau_u \rangle \simeq 377\tau$ for the tetramer. As a result of the

DOI: 10.1021/acs.jpcb.8b10282
J. Phys. Chem. B 2019, 123, 2623−2635

significantly longer unfolding times than for the single-domain SP, on the 500τ timescale of our simulations, the C-terminal domain of multidomain SPs is predominantly found in its native conformation (Figure 2B,C). We also note that limited sampling of unfolded SP conformations with $Q_N < 0.6$ is observed for both dimeric and tetrameric SPs. These longer timescales and less efficient unfolding mechanisms compared with the single-domain SP arise from restricted mobility of the C-terminal I27 domain in multidomain SPs corresponding to orientations largely restricted to angles $\theta \lesssim 40°$ (Figure 2B,C and Supporting Information Movies S3, S4, and S5). To quantitatively characterize these hindered motions of multidomain SPs, we determine the apparent rotational diffusion coefficient for reorientation of the C-terminal I27 domain, prior to the initial unfolding event, with respect to the ClpY pore axis (see Methods). We find that the single-domain I27 SP has an average diffusion coefficient $\langle D \rangle \simeq (4.9 \pm 0.6) \times 10^{-5}$ ps^{-1}, which is slightly lower than the bulk values of unrestrained globular proteins such as bovine pancreatic trypsin inhibitor, $\langle D \rangle \simeq (7.1 \pm 0.1) \times 10^{-5}$ ps^{-1}, and hen white lysozyme $\langle D \rangle \simeq (8.9 \pm 0.1) \times 10^{-5}$ ps^{-1}.[68] By contrast, the dimer and tetramer rotations are more strongly restricted, and the diffusion coefficient is approximately $(1.9 \pm 0.4) \times 10^{-5}$ ps^{-1}. Thus, crowding due to the presence of multiple I27 domains in multidomain SPs in conjunction with SP−ClpY ring interactions hinders the C-terminal domain reorientation along the soft mechanical direction which is associated with efficient unfolding. As shown in Supporting Information illustrating individual dimer and tetramer trajectories, restricted SP orientation and rotational diffusion give rise to two unfolding pathways, one corresponding to shearing at smaller angles, $\theta \lesssim 40°$ (Supporting Information Figure S1B,D and Movies S3 and S5) and another to unzipping mechanism at large angles, $\theta \gtrsim 50°$ (Supporting Information Figure S1C and Movie S4). Long unfolding timescales associated with these mechanisms are due to the slow rotational diffusion of the C-terminal I27 domain. In addition, in the range of low θ angles, long unfolding timescales reflect the high barrier corresponding to cooperative removal of interstrand contacts along the strong mechanical direction parallel to the β-sheet registry.

To assess the effect of the external force used in our model, we performed additional simulations of the SP comprising a single I27 domain in the absence of allosteric conformational transitions of ClpY subunits (Table 1). As shown in Figure 2D and Table 1, no SP unfolding and translocation is observed in simulations of the nonallosteric model, in which the ClpYΔI conformation is restrained near the open configuration (see Methods). We find that the I27 domain samples a broad range of orientations relative to the ClpYΔI surface, as indicated by the broad distribution of the θ values shown in Figure 2D and the Supporting Information Movie S2. These results indicate that the external force alone is insufficient to enable unfolding in the absence of forces generated by the ClpY pore loops. Overall, we surmise that ClpY conformational changes driven by ATP-hydrolysis modulate SP unfolding and translocation through the selection of a favorable SP orientation and immobilization such that the pulling force is applied along the soft mechanical direction perpendicular to the β-sheet registry.

The reorientation of the SP in the plane perpendicular to the ClpY axis reflects the greater mobility of the single-domain substrate on the ATPase surface. As shown in Supporting Information Figure S3A, the projection of the unit vector along the largest principal axis of the C-terminal I27 domain onto this plane (see Methods) has a large magnitude consistent with the tilted orientation of the SP. Large probability densities are concentrated near interfaces between the subunits in the ATP-bound state in the open pore configuration and their clockwise neighbors, as these correspond to the most favorable orientations for gripping the SP. By contrast, dimeric (Supporting Information Figure S3B) and tetrameric (Supporting Information Figure S3C) multidomain SPs strongly restrict the orientation of the C-terminal domain to limited directions, and the magnitude of the projection is reduced. In the absence of allosteric conformational changes of ClpYΔI, the orientation of the I27 domain is largely restricted near the ClpY pore axis.

The interaction of the C-terminal domain with ClpY highlights the efficient unfolding mechanism for the single-domain SP. As shown in Figure 3A, for $t \geq 150\tau$, the average total interaction energy between ClpYΔI and the monomeric SP is approximately $\langle E \rangle \simeq -200 \pm 8$ kcal/mol. By contrast, restricted orientation of the C-terminal domain of multidomain SPs limits its contact with the ClpYΔI surface and results in weaker interaction, with $\langle E \rangle \simeq -167 \pm 12$ kcal/mol for $(I27)_2$ (Figure 3B) and $\langle E \rangle \simeq -151 \pm 12$ kcal/mol for $(I27)_4$ (Figure 3C). In all cases, the van der Waals contribution to the energy dominates, with $\langle E_{vdW} \rangle \simeq -136 \pm 6$ kcal/mol for the monomer, $\simeq -114 \pm 8$ kcal/mol for the dimer, and $\simeq -103 \pm 8$ kcal/mol for the tetramer, which suggests that nonspecific interactions between ClpYΔI and the SP play the primary role. Nevertheless, the electrostatic interaction provides a strong contribution, $\langle E_{el} \rangle \simeq -64 \pm 4$ kcal/mol for the monomer, $\simeq -53 \pm 5$ kcal/mol for the dimer, and $\simeq -48 \pm 5$ kcal/mol for the tetramer, consistent with the important role of the conserved Tyr residue within the central channel loop. In the nonallosteric model (Supporting Information Figure S4A), in which the SP is not in close contact with the Clp pore, the Clp−I27 interaction is significantly weaker than in the allosteric cases, with the average total interaction energy $\langle E \rangle \simeq -88 \pm 9$ kcal/mol, the average van der Waals energy $\langle E_{vdW} \rangle \simeq -56 \pm 6$ kcal/mol, and the average electrostatic energy $\langle E_{el} \rangle \simeq -32 \pm 4$ kcal/mol. Taken together, these results indicate the active role of allosteric conformational transitions of the ATPase in promoting Clp−SP interactions.

External Restraint on N-Terminal Drastically Restricts the SP Orientation and Alters the Unfolding Mechanism. In the restrained geometry, which mimics the setup in LOT experiments, in which an opposing force is applied at the N-terminal (Figure 1), the Clp-mediated force is exerted along the restricted N−C direction. As shown in Figure 2E,F, our simulations, performed using a C-terminal pulling force with an average magnitude of 300 pN and an opposing N-terminal force of 150 pN (Table 1 and Methods), indicating that the rotation of the SP in a plane containing the ClpY axis is severely restricted, and that the polar angle between the largest principal axis of the C-terminal I27 domain and the ClpY pore axis is limited to a small range, $\theta \lesssim 20°$. In addition, the orientation of the I27 domain in the plane perpendicular to the ClpY pore axis is also strongly restricted (Figure S1B,C). Thus, in this geometry, the mechanical strength of the SP is probed along the N−C direction, which corresponds to the direction parallel to the I27 β-sheet registry requiring shearing of the A′−G contacts. Consistently, for the single I27 domain SP, 25 of 36 trajectories result in unfolding with corresponding timescales that are significantly longer than for the unre-

DOI: 10.1021/acs.jpcb.8b10282
J. Phys. Chem. B 2019, 123, 2623−2635

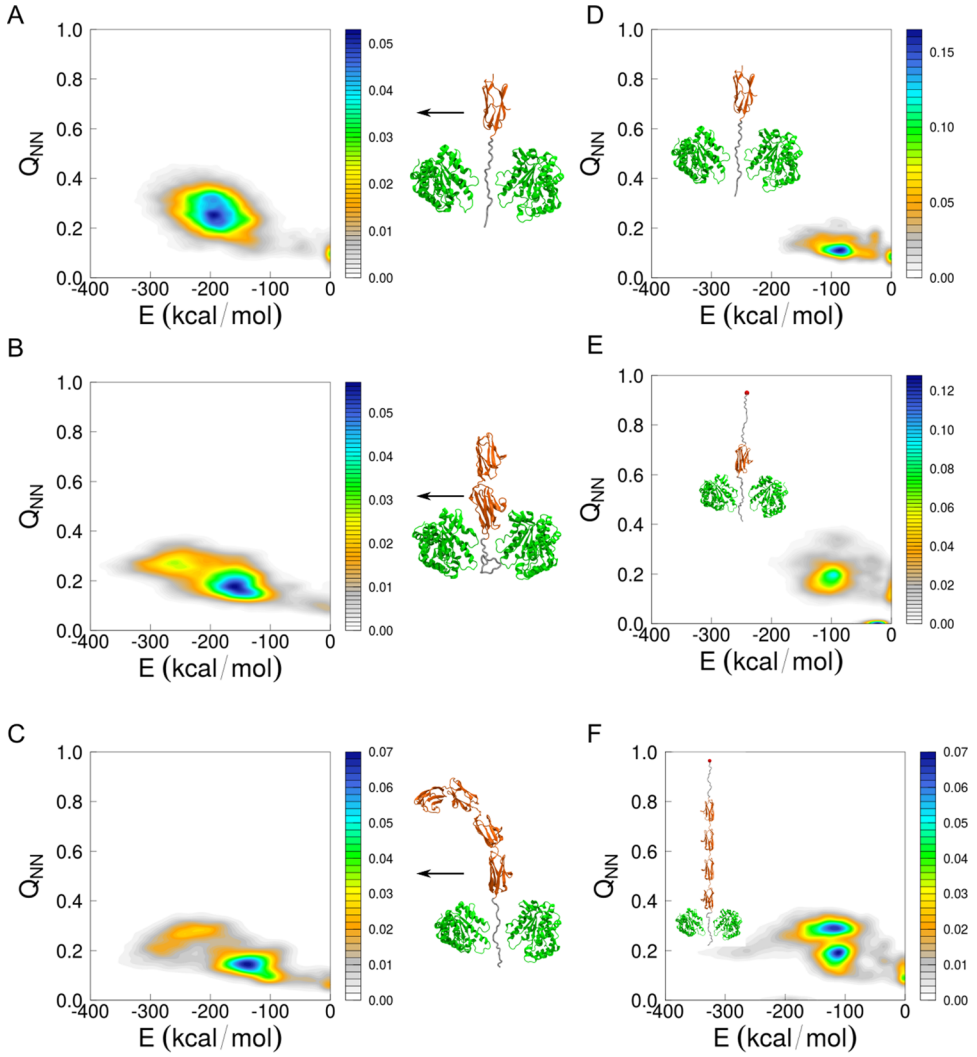

Figure 4. Contribution of non-native contacts to the unfolding of the C-terminal I27 domain. Probability density map of the fraction of non-native contacts, Q_{NN}, and the interaction energy between the untranslocated fragment of the C-terminal I27 domain and the ClpYΔI surface of unrestrained (A) monomeric; (B) dimeric; (C) tetrameric multidomain SPs in allosteric cycles of ClpYΔI. Also shown are the cases of (D) unrestrained monomeric SP and nonallosteric ClpYΔI and restrained (E) monomeric and (F) tetrameric SP and allosteric ClpYΔI.

strained geometry, $\langle \tau_u \rangle \simeq 277\tau$, and the rotational angle is restricted to $\langle \theta \rangle \simeq 10°$ (Figure 2E). The unfolding mechanism corresponds to a two-state transition, consisting of a cooperative removal of nearly all native contacts (Figure 2E and Supporting Information Movie S6). By contrast, weaker propagation of restraining forces along the tetrameric tandem allows slightly greater flexibility of the C-terminal domain, with the rotational angle $\langle \theta \rangle \simeq 15°$, and gives rise to an intermediate unfolded conformation with $\langle Q_N \rangle \simeq 0.75$ on a longer timescale $\langle \tau_u \rangle \simeq 316\tau$ (Figure 2F and Supporting Information Movie S7). Thus, although mechanical forces are applied at N- and C-termini of the tetrameric tandem, straining of the native conformation of the C-terminal I27 domain involves orientations that deviate from the direction of the β-sheet registry. The interaction of the C-terminal domain with ClpY after $t \geq 150\tau$ results in an average total energy $\langle E \rangle \simeq -91 \pm 7$ kcal/mol for the monomer (Supporting Information Figure S4B) and $\langle E \rangle \simeq -116 \pm 11$ kcal/mol for the tetramer (Supporting Information Figure S4C), which are weaker than in the unrestrained cases (Figure 3). These results underscore the less extensive Clp−SP contacts in the restrained geometry due to the limited rotational flexibility of the substrate.

Efficient Remodeling of Unrestrained SP is Modulated by the Formation of Non-Native Contacts. Single-molecule force spectroscopy experiments showed that Clp-mediated degradation of multidomain SPs involves dwell periods corresponding to successive unproductive attempts to unfold individual domains during Clp ATPase power strokes.[7,31−35] Successful unfolding has been attributed to destabilization of the local interface of the SP domain through repetitive Clp-mediated pulling and thermal fluctuations,[31,32] however, a microscopic level understanding of these mechanisms has so far not been available. To reveal the conformational fluctuations of the SP that favor mechanical unfolding, we evaluate the combined probability density distribution of the Cl−SP interaction and the fraction of non-native contacts (see Methods) within the C-terminal I27 domain. As shown in Figure 4A, in the unrestrained geometry, the single-domain I27 SP establishes strong interaction with ClpYΔI, $-250 \lesssim E \lesssim -150$ kcal/mol, which comprises primarily the mechanical pulling exerted by the central channel loops of ClpY onto the C-terminal region of I27. Favorable reorientation of the SP such that the ClpY pore axis is perpendicular to the β-sheet registry, as described above,

DOI: 10.1021/acs.jpcb.8b10282
J. Phys. Chem. B 2019, 123, 2623−2635

allows efficient application of mechanical force by the ClpY loops and results in straining the native contacts within the I27 structure and the formation of a significant fraction of non-native contacts, $0.2 \lesssim Q_{NN} \lesssim 0.4$. Hindered motions of multidomain SPs also result in weaker interactions of native I27 domains with ClpYΔI than in the case of a monomeric SP and fewer non-native contacts formed in the C-terminal domain. We find that, in the dimeric and tetrameric SPs, $-200 \lesssim E \lesssim -100$ kcal/mol with $0.15 \lesssim Q_{NN} \lesssim 0.25$ for the dimer (Figure 4B) and $0.1 \lesssim Q_{NN} \lesssim 0.2$ for the tetramer (Figure 4C). Following the initial unfolding event, increased flexibility of multidomain SPs allows the formation of a larger fraction of non-native contacts, $0.2 \lesssim Q_{NN} \lesssim 0.3$, resulting in stronger SP−ClpY interactions, $-300 \lesssim E \lesssim -200$ kcal/mol (Figure 4B,C). In the absence of allosteric conformational changes, the interaction between the ClpY loops and the monomeric SP results in weak interactions, $-150 \lesssim E \lesssim -50$ kcal/mol, and a smaller fraction of non-native contacts, $Q_{NN} \lesssim 0.15$ (Figure 4D). In the restrained geometry, in accord with the strong directional constraints, we find that non-native contacts have limited contribution to the initial unfolding event, with $0.1 \lesssim Q_{NN} \lesssim 0.2$ and $-150 \lesssim E \lesssim -50$ kcal/mol (Figure 4E,F).

To identify the detailed contribution of non-native contacts to these mechanisms, we examined the time evolution of native and non-native contacts in both unrestrained and restrained geometries of single-domain I27 SPs. Figure 5 shows comparatively the fraction of native and non-native contacts formed by each strand during a single simulation trajectory. In the unrestrained geometry, rapid reorientation and conformational fluctuations of the SP on the ClpYΔI surface result in a large increase of the number of non-native contacts of SP prior to completion of the N → I1 unfolding step at $t \lesssim 230\tau$ (Figure 5A). As a result of repetitive ClpY−SP interactions, gradual loss of native contacts occurs at the A′ strand and at the distal C and D strands. Thus, the destabilization mechanism of the native SP structure in allosteric cycles of ClpY involves loss of native contacts at both A′−G and C−D strand pairs that bound the two β-sheets of I27. Distortion of the SP structure facilitates the formation of non-native contacts at the A′−G interface and at the distal C strand (Figure 5A). As the unfolding of the unrestrained monomer occurs on a fast timescale compared with the restrained case, we propose that non-native interactions provide the on-pathway contribution to domain unfolding. In accord with the above observations, the ensemble-averaged results, shown in Figure S5A, indicate that within the timescale of the initial unfolding, $\langle \tau_u \rangle \lesssim 112\tau$, the destabilization mechanism of the native conformation consists in gradual replacement of A′−G and C−D native contacts with non-native contacts. In contrast to these mechanisms, unfolding of the restrained SP does not involve a significant contribution from non-native contacts prior to the initial unfolding at $\tau_u \simeq 130\tau$. As the SP reorientation is limited and the force is applied along the restricted N−C direction, SP unfolding occurs through cooperative removal of A′−G contacts, which precludes the formation of non-native contacts (Figure 5B). The ensemble-averaged results, shown in Figure S5B, also indicate a small contribution of non-native interactions to the unfolding in the restrained geometry. On the timescale of the initial unfolding event, $\langle \tau_u \rangle \lesssim 277\tau$, non-negligible formation of non-native contacts only involves the C strand. We note, however, that, in the ensemble-average, the fraction of non-native contacts involving the C strand includes contributions from both native and unfolded conformations of

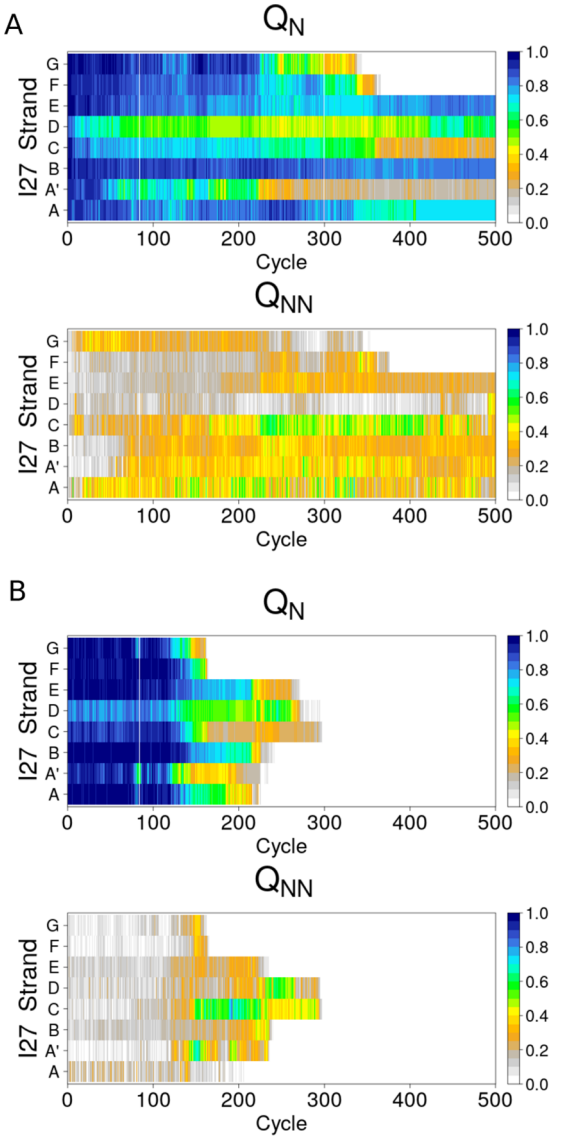

Figure 5. Relative contribution of local native and non-native contacts to the unfolding of the C-terminal I27 domain. Time evolution of the fraction of native (upper panel) and non-native (lower panel) contacts of individual strands of I27 in the monomeric SP is shown for a single trajectory of Clp-mediated I27 unfolding in (A) unrestrained and (B) restrained cases.

I27 as the individual unfolding events are broadly distributed on this timescale, and a significant reduction of the fraction of native contacts occurs (Supporting Information Figure S5B). Overall, these results indicate that the formation of non-native contacts is favored in the unrestrained geometries that enable SP flexibility. This facilitates weakening of soft mechanical interfaces thereby increasing the efficacy of the unfolding mechanisms.

DISCUSSION AND CONCLUSIONS

Our computational study reveals that mechanisms of Clp-mediated degradation are strongly affected by the presence of multiple protomers in a multidomain SP. We find that unfolding of SPs comprising a single I27 protomer involves its reorientation such that the Clp-mediated pulling force is applied along a soft mechanical direction. The lower energy barrier associated with this weaker mechanical direction

DOI: 10.1021/acs.jpcb.8b10282
J. Phys. Chem. B 2019, 123, 2623−2635

combined with the rapid SP rotation yields SP degradation on a fast timescale. By contrast, for SPs that include 2 or 4 protomers, interdomain and domain-Clp surface interactions hinder rotational diffusion of the C-terminal domain and result in slower unfolding. In addition, high mechanical anisotropy of the I27 domain gives rise to a second unfolding pathway involving a strong mechanical direction. Thus, SP tandems that comprise multiple protomers have longer unfolding timescales and distinct direction-dependent mechanisms. We also find that non-native interactions modulate these mechanisms by weakening the mechanical resistance of interfaces being pulled. Further insight into the degradation of multidomain SPs is likely to emerge from considering heterogeneous protomers. For example, bulky protomers may severely restrict the rotational motion of C-terminal domains, thereby selecting limiting force application along specific directions. Overall, we propose that kinetic effects that hinder access to the soft mechanical interface of the C-terminal domain, coupled with the transient SP gripping by the ATPase, result in the release of undegraded fragments comprising folded domains.

Other types of interdomain interactions that may affect degradation rates of multidomain SPs are those arising in endoproteolytic mechanisms, disaggregation, and interaction with auxiliary domains of AAA+ machinery. Endoproteolytic mechanisms involve specific mechanisms of the unfolding of multidomain SPs due to AAA-mediated mechanical pulling on an internal loop connecting two folded domains.[69−72] The interplay between force directionality and mechanical resistance of the N- and C-terminal regions flanking the loop should yield complex domain-dependent unfolding mechanisms that include complete or partial degradation of SP domains. Indeed, recent experimental results give strong support to an interdomain stabilization mechanism.[69] Hindered rotation is likely to play an important role through steric or attractive interactions between the folded domains, therefore the unfolding mechanisms of each domain may involve distinct interfaces compared with the single-domain SPs. In addition, degradation rates can be decreased due to the requirement of simultaneous translocation of the double polypeptide chain and the less frequent force application to the weaker mechanical interface.

Auxiliary domains, such as the I-domains of ClpY and N-domains of ClpX or ClpB, are located on the proximal side of the translocation channel and endow AAA+ machines with specific SP handling actions. These domains modulate SP unfolding mechanisms either through SP confinement, which restricts the available conformational space, or through SP binding, which stabilizes domain configurations. Both actions are highly dynamic due to the large conformational flexibility of auxiliary domains and should result in probing mechanical resistance of the SP domains along selective directions. Notably, these actions may lead to increased or decreased degradation rates depending on the favored domain orientations.[48,73−77]

In AAA+-mediated disaggregation, remodeling action is likely to result in distinct pathways associated with multidomain SPs as interdomain interfaces are stabilized by extensive noncovalent interactions, therefore disruption of these interfaces requires large mechanical forces. This action is performed by machines such as the bacterial ClpB ATPase and its eukaryotic homolog Hsp104. Interestingly, recent studies revealed a spiral arrangement of Hsp104 subunits and a ratcheting SP translocation mechanism that contrast the planar structure of ClpX or ClpY and their power stroke action.[78−81] Continuous gripping of the SP in the Hsp104-mediated action combined with the large-scale deformation of the AAA+ ring should result in distinct constraints applied onto the SP rotational motion and therefore result in specific unfolding mechanisms.

■ ASSOCIATED CONTENT

Supporting Information

The Supporting Information is available free of charge on the ACS Publications website at DOI: 10.1021/acs.jpcb.8b10282.

Time-dependent orientation and fraction of native contacts of the C-terminal I27 domain (Figure S1); unfolding and orientation of the monomeric SP in simulations of unrestrained and restrained geometries using longer cycle durations (Figure S2); orientation of the C-terminal I27 domain on the ClpYΔI surface (Figure S3); interaction between the C-terminal I27 domain and ClpYΔI in nonallosteric pore and restrained geometries (Figure S4); ensemble-averaged relative contribution of local native and non-native contacts to the unfolding of the C-terminal I27 domain (Figure S5) (PDF)

Movie S1 showing molecular simulation of unfolding and translocation of an unrestrained monomeric SP in allosteric cycles of ClpYΔI (green), with SP comprising one titin I27 domain (orange) and $(SsrA)_2$ peptides (gray) (AVI)

Movie S2 showing molecular simulation of unfolding and translocation of an unrestrained monomeric SP and non-allosteric ClpYΔI (AVI)

Movie S3 showing molecular simulation of unfolding and translocation of unrestrained dimeric SP which unfolds through a shearing mechanism (AVI)

Movie S4 showing molecular simulation of unfolding and translocation of an unrestrained dimeric SP which unfolds through an unzipping mechanism (AVI)

Movie S5 showing molecular simulation of unfolding and translocation of unrestrained tetrameric SP (AVI)

Movie S6 showing molecular simulation of unfolding and translocation for a restrained monomeric SP (AVI)

Movie S7 showing molecular simulation of unfolding and translocation for a restrained tetrameric SP (AVI)

■ AUTHOR INFORMATION

Corresponding Author

*E-mail: george.stan@uc.edu. Phone: +1 (513) 556-3049. Fax: +1 (513) 556-9239.

ORCID

George Stan: 0000-0003-1880-4173

Present Address

§Discovery, Product Development & Supply, Janssen Research & Development, Spring House, Pennsylvania 19477, United States (A.J.)

Notes

The authors declare no competing financial interest.

■ ACKNOWLEDGMENTS

The authors thank Sue Wickner, Michael Maurizi, Matthew Lang, and Tania Baker for extensive discussions. This work has been supported by the National Science Foundation (NSF)

DOI: 10.1021/acs.jpcb.8b10282
J. Phys. Chem. B 2019, 123, 2623−2635

grant MCB-1516918 to G.S. Partial support for S.M.F. was provided through the NSF Research Experience for Undergraduates in Chemistry grant CHE-1659648. This work used the Extreme Science and Engineering Discovery Environment (XSEDE), which is supported by NSF grant number ACI-1548562. XSEDE Comet resources were used at the San Diego Supercomputer Center through allocation TG-MCB170020 to G.S.

REFERENCES

(1) Flynn, J. M.; Neher, S. B.; Kim, Y.; Sauer, R. T.; Baker, T. A. Proteomic Discovery of Cellular Substrates of the ClpXP Protease Reveals Five Classes of ClpX-Recognition Signals. *Mol. Cell* **2003**, *11*, 671−683.

(2) Hinnerwisch, J.; Fenton, W. A.; Furtak, K. J.; Farr, G. W.; Horwich, A. L. Loops in the Central Channel of ClpA Chaperone Mediate Protein Binding, Unfolding, and Translocation. *Cell* **2005**, *121*, 1029−1041.

(3) Martin, A.; Baker, T. A.; Sauer, R. T. Pore loops of the AAA+ ClpX machine grip substrates to drive translocation and unfolding. *Nat. Struct. Mol. Biol.* **2008**, *15*, 1147−1151.

(4) Martin, A.; Baker, T.; Sauer, R. Diverse pore loops of the AAA plus ClpX machine mediate unassisted and adaptor-dependent recognition of ssrA-tagged substrates. *Mol. Cell* **2008**, *29*, 441−450.

(5) Lee, C.; Schwartz, M. P.; Prakash, S.; Iwakura, M.; Matouschek, A. ATP-Dependent Proteases Degrade Their Substrates by Processively Unraveling Them from the Degradation Signal. *Mol. Cell* **2001**, *7*, 627−637.

(6) Kenniston, J. A.; Baker, T. A.; Sauer, R. T. Partitioning between unfolding and release of native domains during ClpXP degradation determines substrate selectivity and partial processing. *Proc. Natl. Acad. Sci. U.S.A.* **2005**, *102*, 1390−1395.

(7) Sen, M.; Maillard, R.; Nyquist, K.; Rodriguez-Aliaga, P.; Pressé, S.; Martin, A.; Bustamante, C. The ClpXP Protease Unfolds Substrates Using a Constant Rate of Pulling but Different Gears. *Cell* **2013**, *155*, 636−646.

(8) Maurizi, M.; Stan, G. ClpX Shifts into High Gear to Unfold Stable Proteins. *Cell* **2013**, *155*, 502−504.

(9) Kenniston, J. A.; Baker, T. A.; Fernandez, J. M.; Sauer, R. T. Linkage between ATP Consumption and Mechanical Unfolding during the Protein Processing Reactions of an AAA+ Degradation Machine. *Cell* **2003**, *114*, 511−520.

(10) Palombella, V. J.; Rando, O. J.; Goldberg, A. L.; Maniatis, T. The ubiquitin-proteasome pathway is required for processing the NF-κB1 precursor protein and the activation of NF-κB. *Cell* **1994**, *78*, 773−785.

(11) Lin, L.; Ghosh, S. A glycine-rich region in NF-kappaB p105 functions as a processing signal for the generation of the p50 subunit. *Mol. Cell. Biol.* **1996**, *16*, 2248−2254.

(12) Aza-Blanc, P.; Ramírez- Weber, F. A.; Laget, M. P.; Schwartz, C.; Kornberg, T. B. Proteolysis that is inhibited by hedgehog targets cubitus interruptus protein to the nucleus and converts it to a repressor. *Cell* **1997**, *89*, 1043−1053.

(13) Hoppe, T.; Matuschewski, K.; Rape, M.; Schlenker, S.; Ulrich, H. D.; Jentsch, S. Activation of a Membrane-Bound Transcription Factor by Regulated Ubiquitin/Proteasome-Dependent Processing. *Cell* **2000**, *102*, 577−586.

(14) Wang, B.; Fallon, J. F.; Beachy, P. A. Hedgehog-Regulated Processing of Gli3 Produces an Anterior/Posterior Repressor Gradient in the Developing Vertebrate Limb. *Cell* **2000**, *100*, 423−434.

(15) Rape, M.; Jentsch, S. Taking a bite: proteasomal protein processing. *Nat. Cell Biol.* **2002**, *4*, E113−E116.

(16) Tian, L.; Holmgren, R. A.; Matouschek, A. A conserved processing mechanism regulates the activity of transcription factors Cubitus interruptus and NF-κB. *Nat. Struct. Mol. Biol.* **2005**, *12*, 1045−1053.

(17) Pan, Y.; Bai, C. B.; Joyner, A. L.; Wang, B. Sonic hedgehog Signaling Regulates Gli2 Transcriptional Activity by Suppressing Its Processing and Degradation. *Mol. Cell. Biol.* **2006**, *26*, 3365−3377.

(18) Orian, A.; Schwartz, A. L.; Israël, A.; Whiteside, S.; Kahana, C.; Ciechanover, A. Structural motifs involved in ubiquitin-mediated processing of the NF-kappaB precursor p105: roles of the glycine-rich region and a downstream ubiquitination domain. *Mol. Cell. Biol.* **1999**, *19*, 3664−73.

(19) Tempé, D.; Casas, M.; Karaz, S.; Blanchet-Tournier, M.-F.; Concordet, J.-P. Multisite Protein Kinase A and Glycogen Synthase Kinase 3β Phosphorylation Leads to Gli3 Ubiquitination by $SCF^{\beta TrCP}$. *Mol. Cell. Biol.* **2006**, *26*, 4316−4326.

(20) Jiang, Y. Regulation of the Cell Cycle by Protein Phosphatase 2A in Saccharomyces cerevisiae. *Cell Cycle* **2006**, *70*, 440−449.

(21) Vass, R. H.; Chien, P. Critical clamp loader processing by an essential AAA+ protease in Caulobacter crescentus. *Proc. Natl. Acad. Sci. U.S.A.* **2013**, *110*, 18138−18143.

(22) Virnau, P.; Mirny, L. A.; Kardar, M. Intricate knots in proteins: Function and evolution. *PLoS Comput. Biol.* **2006**, *2*, No. e122.

(23) Huang, L.; Makarov, D. E. Translocation of a knotted polypeptide through a pore. *J. Chem. Phys.* **2008**, *129*, No. 121107.

(24) Szymczak, P. Tight knots in proteins: can they block the mitochondrial pores? *Biochem. Soc. Trans.* **2013**, *41*, 620−4.

(25) Szymczak, P. Translocation of knotted proteins through a pore. *Eur. Phys. J.: Spec. Top.* **2014**, *223*, 1805−1812.

(26) Szymczak, P. Periodic forces trigger knot untying during translocation of knotted proteins. *Sci. Rep.* **2016**, *6*, No. 21702.

(27) Rosa, A.; Ventra, M. D.; Micheletti, C. Topological Jamming of Spontaneously Knotted Polyelectrolyte Chains Driven Through a Nanopore. *Phys. Rev. Lett.* **2012**, *109*, No. 118301.

(28) Wojciechowski, M.; Gómez-Sicilia, À.; Carrión-Vázquez, M.; Cieplak, M. Unfolding knots by proteasome-like systems: simulations of the behaviour of folded and neurotoxic proteins. *Mol. BioSyst.* **2016**, *12*, 2700−2712.

(29) San Martín, Á.; Rodriguez-Aliaga, P.; Molina, J. A.; Martin, A.; Bustamante, C.; Baez, M. Knots can impair protein degradation by ATP-dependent proteases. *Proc. Natl. Acad. Sci. U.S.A.* **2017**, *114*, 9864.

(30) Zhmurov, A.; Dima, R. I.; Barsegov, V. Order statistics theory of unfolding of multimeric proteins. *Biophys. J.* **2010**, *99*, 1959−1968.

(31) Aubin-Tam, M.-E.; Olivares, A.; Sauer, R.; Baker, T.; Lang, M. Single-Molecule Protein Unfolding and Translocation by an ATP-Fueled Proteolytic Machine. *Cell* **2011**, *145*, 257−267.

(32) Maillard, R.; Chistol, G.; Sen, M.; Righini, M.; Tan, J.; Kaiser, C. M.; Hodges, C.; Martin, A.; Bustamante, C. ClpX(P) Generates Mechanical Force to Unfold and Translocate Its Protein Substrates. *Cell* **2011**, *145*, 459−469.

(33) Cordova, J.; Olivares, A.; Shin, Y.; Stinson, B.; Calmat, S.; Schmitz, K.; Aubin-Tam, M.-E.; Baker, T.; Lang, M.; Sauer, R. Stochastic but Highly Coordinated Protein Unfolding and Translocation by the ClpXP Proteolytic Machine. *Cell* **2014**, *158*, 647−658.

(34) Olivares, A. O.; Nager, A. R.; Iosefson, O.; Sauer, R. T.; Baker, T. A. Mechanochemical basis of protein degradation by a double-ring AAA+ machine. *Nat. Struct. Mol. Biol.* **2014**, *21*, 871−875.

(35) Olivares, A. O.; Kotamarthi, H. C.; Stein, B. J.; Sauer, R. T.; Baker, T. A. Effect of directional pulling on mechanical protein degradation by ATP-dependent proteolytic machines. *Proc. Natl. Acad. Sci. U.S.A.* **2017**, *114*, E6306−E6313.

(36) Carrion-Vazquez, M.; Oberhauser, A. F.; Fowler, S. B.; Marszalek, P. E.; Broedel, S. E.; Clarke, J.; Fernandez, J. M. Mechanical and Chemical Unfolding of a Single Protein: A Comparison. *Proc. Natl. Acad. Sci. U.S.A.* **1999**, *96*, 3694−3699.

(37) Li, H.; Carrión-Vázquez, M.; Oberhauser, A. F.; Marszalek, P. E.; Fernandez, J. M. Point mutations alter the mechanical stability of immunoglobulin modules. *Nat. Struct. Biol.* **2000**, *7*, 1117−1120.

(38) Lu, H.; Schulten, K. The key event in force-induced unfolding of Titin's immunoglobulin domains. *Biophys. J.* **2000**, *79*, 51−65.

(39) Fowler, S. B.; Best, R. B.; Toca Herrera, J. L.; Rutherford, T. J.; Steward, A.; Paci, E.; Karplus, M.; Clarke, J. Mechanical unfolding of a

DOI: 10.1021/acs.jpcb.8b10282
J. Phys. Chem. B 2019, 123, 2623−2635

titin Ig domain: Structure of unfolding intermediate revealed by combining AFM, molecular dynamics simulations, NMR and protein engineering. *J. Mol. Biol.* **2002**, *322*, 841−849.
(40) Best, R. B.; Fowler, S. B.; Herrera, J. L.; Steward, A.; Paci, E.; Clarke, J. Mechanical Unfolding of a Titin Ig Domain: Structure of Transition State Revealed by Combining Atomic Force Microscopy, Protein Engineering and Molecular Dynamics Simulations. *J. Mol. Biol.* **2003**, *330*, 867−877.
(41) West, D. K.; Brockwell, D. J.; Paci, E. Prediction of the Translocation Kinetics of a Protein from Its Mechanical Properties. *Biophys. J.* **2006**, *91*, L51−L53.
(42) West, D.; Olmsted, P.; Paci, E. Mechanical unfolding revisited through a simple but realistic model. *J. Chem. Phys.* **2006**, *124*, No. 154909.
(43) Duan, L.; Zhmurov, A.; Barsegov, V.; Dima, R. I. Exploring the mechanical stability of the C2 domains in human synaptotagmin 1. *J. Phys. Chem. B* **2011**, *115*, 10133−10146.
(44) Wojciechowski, M.; Szymczak, P.; Carrión-Vázquez, M.; Cieplak, M. Protein Unfolding by Biological Unfoldases: Insights from Modeling. *Biophys. J.* **2014**, *107*, 1661−1668.
(45) Lazaridis, T.; Karplus, M. Effective Energy Function for Proteins in Solution. *Proteins: Struct., Funct., Genet.* **1999**, *35*, 133−152.
(46) Masunov, A.; Lazaridis, T. Potentials of mean force between ionizable amino acid side chains in water. *J. Am. Chem. Soc.* **2003**, *125*, 1722−1730.
(47) Huang, L.; Kirmizialtin, S.; Makarov, D. E. Computer simulations of the translocation and unfolding of a protein pulled mechanically through a pore. *J. Chem. Phys.* **2005**, *123*, No. 124903.
(48) Kravats, A.; Jayasinghe, M.; Stan, G. Unfolding and translocation pathway of substrate protein controlled by structure in repetitive allosteric cycles of the ClpY ATPase. *Proc. Natl. Acad. Sci. U.S.A.* **2011**, *108*, 2234−2239.
(49) Kravats, A. N.; Tonddast-Navaei, S.; Bucher, R. J.; Stan, G. Asymmetric processing of a substrate protein in sequential allosteric cycles of AAA+ nanomachines. *J. Chem. Phys.* **2013**, *139*, No. 121921.
(50) Tonddast-Navaei, S.; Stan, G. Mechanism of Transient Binding and Release of Substrate Protein during the Allosteric Cycle of the p97 Nanomachine. *J. Am. Chem. Soc.* **2013**, *135*, 14627−14636.
(51) Kravats, A. N.; Tonddast-Navaei, S.; Stan, G. Coarse-Grained Simulations of Topology-Dependent Mechanisms of Protein Unfolding and Translocation Mediated by ClpY ATPase Nanomachines. *PLoS Comput. Biol.* **2016**, *12*, No. e1004675.
(52) Javidialesaadi, A.; Stan, G. Asymmetric Conformational Transitions in AAA+ Biological Nanomachines Modulate Direction-Dependent Substrate Protein Unfolding Mechanisms. *J. Phys. Chem. B* **2017**, *121*, 7108−7121.
(53) Luan, B.; Huynh, T.; Li, J.; Zhou, R. Nanomechanics of Protein Unfolding Outside a Generic Nanopore. *ACS Nano* **2016**, *10*, 317−323.
(54) Humphrey, W.; Dalke, A.; Schulten, K. VMD - Visual Molecular Dynamics. *J. Mol. Graphics* **1996**, *14*, 33−38.
(55) van der Vaart, A.; Ma, J.; Karplus, M. The Unfolding Action of GroEL on a Protein Substrate. *Biophys. J.* **2004**, *87*, 562−573.
(56) Improta, S.; Politou, A. S.; Pastore, A. Immunoglobulin-Like Modules from Titin I-Band: Extensible Components of Muscle Elasticity. *Structure* **1996**, *4*, 323−337.
(57) Brooks, B. R.; Brooks, C. L.; Mackerell, A. D.; Nilsson, L.; Petrella, R. J.; Roux, B.; Won, Y.; Archontis, G.; Bartels, C.; Boresch, S.; et al. CHARMM: the biomolecular simulation program. *J. Comput. Chem.* **2009**, *30*, 1545−1614.
(58) Towns, J.; Cockerill, T.; Dahan, M.; Foster, I.; Gaither, K.; Grimshaw, A.; Hazlewood, V.; Lathrop, S.; Lifka, D.; Peterson, G. D.; et al. XSEDE: Accelerating Scientific Discovery. *Comput. Sci. Eng.* **2014**, *16*, 62−74.
(59) Schlitter, J.; Engels, M.; Kruger, P.; Jacoby, E. U.; Wollmer, A. Targeted molecular dynamics simulation of conformational change: application to the T-R transition in insulin. *Mol. Simul.* **1993**, *10*, 291−308.
(60) Keskin, O.; Bahar, I.; Flatow, D.; Covell, D. G.; Jernigan, R. L. Molecular Mechanisms of Chaperonin GroEL-GroES Function. *Biochemistry* **2002**, *41*, 491−501.
(61) Zheng, W.; Brooks, B. R.; Thirumalai, D. Allosteric transitions in the chaperonin GroEL are captured by a dominant normal mode that is most robust to sequence variations. *Biophys. J.* **2007**, *93*, 2289−2299.
(62) Tehver, R.; Chen, J.; Thirumalai, D. Allostery Wiring Diagrams in the Transitions that Drive the GroEL Reaction Cycle. *J. Mol. Biol.* **2009**, *387*, 390−406.
(63) Skjaerven, L.; Grant, B.; Muga, A.; Teigen, K.; McCammon, J. A.; Reuter, N.; Martinez, A. Conformational sampling and nucleotide-dependent transitions of the GroEL subunit probed by unbiased molecular dynamics simulations. *PLoS Comput. Biol.* **2011**, *7*, No. e1002004.
(64) Abrams, C. F.; Vanden-Eijnden, E. Large-scale conformational sampling of proteins using temperature-accelerated molecular dynamics. *Proc. Natl. Acad. Sci. U.S.A.* **2010**, *107*, 4961−4966.
(65) Bochtler, M.; Hartmann, C.; Song, H. K.; Bourenkov, G. P.; Bartunik, H. D.; Huber, R. The structures of HslU and the ATP-dependent protease HslU-HslV. *Nature* **2000**, *403*, 800−805.
(66) Ma, J.; Sigler, P. B.; Xu, Z. H.; Karplus, M. A dynamic model for allosteric mechanism for GroEL. *J. Mol. Biol.* **2000**, *302*, 303−313.
(67) Nam, K.; Pu, J.; Karplus, M. Trapping the ATP binding state leads to a detailed understanding of the F1 -ATPase mechanism. *Proc. Natl. Acad. Sci. U.S.A.* **2014**, *111*, 17851−17856.
(68) Smith, P. E.; van Gunsteren, W. F. Translational and rotational diffusion of proteins. *J. Mol. Biol.* **1994**, *236*, 629−636.
(69) Kraut, D. A.; Matouschek, A. Proteasomal Degradation from Internal Sites Favors Partial Proteolysis via Remote Domain Stabilization. *ACS Chem. Biol.* **2011**, *6*, 1087−1095.
(70) Kraut, D. A.; Israeli, E.; Schrader, E. K.; Patil, A.; Nakai, K.; Nanavati, D.; Inobe, T.; Matouschek, A. Sequence- and species-dependence of proteasomal processivity. *ACS Chem. Biol.* **2012**, *7*, 1444−1453.
(71) Fishbain, S.; Prakash, S.; Herrig, A.; Elsasser, S.; Matouschek, A. Rad23 escapes degradation because it lacks a proteasome initiation region. *Nat. Commun.* **2011**, *2*, No. 192.
(72) Fishbain, S.; Inobe, T.; Israeli, E.; Chavali, S.; Yu, H.; Kago, G.; Babu, M. M.; Matouschek, A. Sequence composition of disordered regions fine-tunes protein half-life. *Nat. Struct. Mol. Biol.* **2015**, *22*, 214−221.
(73) Dougan, D. A.; Weber-Ban, E.; Bukau, B. Targeted Delivery of an SsrA-Tagged Substrate by the Adaptor Protein SspB to its Cognate AAA+ Protein ClpX. *Mol. Cell* **2003**, *12*, 373−380.
(74) Cranz-Mileva, S.; Imkamp, F.; Kolygo, K.; Maglica, Ž.; Kress, W.; Weber-Ban, E. The Flexible Attachment of the N-Domains to the ClpA Ring Body Allows their Use On Demand. *J. Mol. Biol.* **2008**, *378*, 412−424.
(75) Doyle, S. M.; Hoskins, J. R.; Wickner, S. DnaK Chaperone-Dependent Disaggregation by Caseinolytic Peptidase B (ClpB) Mutants Reveals Functional Overlap in the N-terminal Domain and Nucleotide-Binding Domain-1 Pore Tyrosine. *J. Biol. Chem.* **2012**, *287*, 28470−28479.
(76) Sundar, S.; Baker, T.; Sauer, R. The I domain of the AAA+ HsIUV protease coordinates substrate binding, ATP hydrolysis, and protein degradation. *Protein Sci.* **2012**, *21*, 188−198.
(77) Sweeny, E. A.; Jackrel, M. E.; Go, M. S.; Sochor, M. A.; Razzo, B. M.; DeSantis, M. E.; Gupta, K.; Shorter, J. The Hsp104 N-Terminal Domain Enables Disaggregase Plasticity and Potentiation. *Mol. Cell* **2015**, *57*, 836−849.
(78) Yokom, A. L.; Gates, S. N.; Jackrel, M. E.; Mack, K. L.; Su, M.; Shorter, J.; Southworth, D. R. Spiral architecture of the Hsp104 disaggregase reveals the basis for polypeptide translocation. *Nat. Struct. Mol. Biol.* **2016**, *23*, 830−837.
(79) Gates, S. N.; Yokom, A. L.; Lin, J.; Jackrel, M. E.; Rizo, A. N.; Kendsersky, N. M.; Buell, C. E.; Sweeny, E. A.; Mack, K. L.; Chuang, E.; et al. Ratchet-like polypeptide translocation mechanism of the AAA+ disaggregase Hsp104. *Science* **2017**, *357*, 273−279.

DOI: 10.1021/acs.jpcb.8b10282
J. Phys. Chem. B 2019, 123, 2623−2635

(80) Deville, C.; Carroni, M.; Franke, K. B.; Topf, M.; Bukau, B.; Mogk, A.; Saibil, H. R. Structural pathway of regulated substrate transfer and threading through an Hsp100 disaggregase. *Sci. Adv.* **2017**, *3*, No. e1701726.
(81) Yu, H.; Lupoli, T. J.; Kovach, A.; Meng, X.; Zhao, G.; Nathan, C. F.; Li, H. ATP hydrolysis-coupled peptide translocation mechanism of Mycobacterium tuberculosis ClpB. *Proc. Natl. Acad. Sci. U.S.A.* **2018**, *115*, E9560−E9569.

DOI: 10.1021/acs.jpcb.8b10282
J. Phys. Chem. B 2019, 123, 2623−2635